Atmospheric Research 153 (2015) 235–249

Contents lists available at ScienceDirect

Atmospheric Research

journal homepage: www.elsevier.com/locate/atmos

A study of aerosol optical properties during ozone pollution episodes in 2013 over Shanghai, China

Chanzhen Shi [a], Shanshan Wang [c], Rui Liu [a,d], Rui Zhou [a], Donghui Li [b], Wenxin Wang [a], Zhengqiang Li [b], Tiantao Cheng [a,e], Bin Zhou [a,e,*]

[a] Shanghai Key Laboratory of Atmospheric Particle Pollution and Prevention (LAP^3), Department of Environmental Science and Engineering, Fudan University, Shanghai, China
[b] State Environmental Protection Key laboratory of Satellites Remote Sensing, Institute of Remote Sensing and Digital Earth of Chinese Academy of Sciences, Beijing, China
[c] School of Environment and Architecture, University of Shanghai for Science and Technology, Shanghai 200093, China
[d] Department of Geographic Information Science, Yunan University, Kunming 650091, China
[e] Fudan-Tyndall Centre, Fudan University, Shanghai 200433, China

ARTICLE INFO

Article history:
Received 9 May 2014
Received in revised form 12 July 2014
Accepted 3 September 2014
Available online 9 September 2014

Keywords:
Aerosol
Ozone pollution
Optical property
Extinction profile
Shanghai

ABSTRACT

Aerosol optical property is essential to the tropospheric ozone formation mechanism while it was rarely measured in ozone-rich environment for a specific study. With the retrieved products of the sun-photometer, a comparative investigation was conducted on aerosol optical depth (AOD), single scattering albedo (SSA) and size distribution during ozone-polluted episodes and clean background. Contrary to expectations, aerosol loading was found to be positively-correlated with ozone concentration: daily averaged AOD at 500 nm in ozone episodes (~0.78) displayed 2.4 times higher than that in clean days (~0.32). Large Ångström exponent (~1.51) along with heavy aerosol loading indicated a considerable impact of fine particles on optical extinction. The dynamic diurnal fluctuation of these parameters also implied a complex interaction between aerosols and photo-chemical reactions. The bimodal lognormal distribution pattern for aerosol size spectra exhibited in both ozone-polluted and clean days. The occurrence of maximum volume concentration (~0.28) in fine mode (radius <0.6 μm) was observed at 3 p.m. (local time), when ozone was substantially generated. Pronounced scattering feature of aerosol was reproduced in high-concentration ozone environment. SSA tended to increase continuously from morning (~0.91 at 440 nm) to afternoon (~0.99), which may be associated with secondary aerosol formation. The scattering aerosol (with moderately high aerosol loading) may favor the ozone formation through increasing solar flux in boundary layer. Utilizing the micro-pulse lidar (MPL), a more developed planet boundary layer (PBL, top height ~1.96 km) was discovered during ozone-polluted days than clean condition (~1.4 km). In episodes, the maximum extinction ratio (~0.5 km^{-1}) was presented at a height of 1.2 km in the late afternoon. The humidity profile by sounding also showed the extreme value at this altitude. It suggested that optical extinction was mainly attributed to the aerosol in middle PBL, where the intense photochemical reactions and hydroscopic growth may occur.

1. Introduction

Preceded with nitrogen oxides (NO_x) and non-methane organic compounds (NMHC), ozone (O_3) on the Earth's surface is regarded as a secondary pollutant endangering ecosystem (Lippmann, 1995; McMurry and Stolzenburg, 1989; Thurston and Ito, 2000). Concerning the generation and depletion

* Corresponding author at: Shanghai Key Laboratory of Atmospheric Particle Pollution and Prevention (LAP^3), Department of Environmental Science and Engineering, Fudan University, Shanghai, China. Tel.: +86 13 816823197; fax: +86 21 65642530.
E-mail address: binzhou@fudan.edu.cn (B. Zhou).

http://dx.doi.org/10.1016/j.atmosres.2014.09.002
0169-8095/

mechanism, studies have illustrated tropospheric ozone as a non-linear function of primary emission, secondary formation, aerosol interactions, meteorological elements (mainly including temperature, solar radiation and relative humidity), regional transport, vertical distribution and sinks (including reductions and deposition) (Cheung and Wang, 2005; Logan, 1985; Bonn and Moorgat, 2002; Guo et al., 2012; Jenkin and Clemitshaw, 2000; Zuend and Seinfeld, 2012). Atmospheric aerosols exert a convoluted modification on climate changes/radiative forcing and environment via scattering and absorbing light from ultraviolet (UV) to near infrared (NIR) band (IPCC, 2001; Zhou and Savijärvi, 2014; Li et al., 2014). Considering the impact on solar radiation, the presence of aerosol loading has an impressive influence on the photolysis rates of NO_x and O_3, which could further determine the formation and depletion of ozone (He and Carmichael, 1999; Varotsos, 2005). Human activities have been proved to be responsible for the increasing amount of ozone, its precursors and tropospheric aerosols (Dubovik and King, 2000; Pozzoli et al., 2011).

It is well agreed that the variable aerosol properties considerably complicate the ozone formation and depletion process (Hofmann et al., 1994; Kroll et al., 2006; Ran et al., 2009; Varotsos, 2005; O'Dowd et al., 2010). Lou et al. (2014) found that ozone concentration in China underwent about 9% and 33% increase with and without the impact of anthropogenic aerosols. In detail, two prominent ways are classified as the aerosol's impact on ozone: modifying heterogeneous reactions and altering photolysis rates (of ozone and its precursory) by aerosol–radiation interactions (Geng et al., 2007; Jacobson, 1998). Via heterogeneous reactions, aerosols can uptake NO_3 and NO_2 while increase OH radicals, consequently leading to ozone variations (Li et al., 2014; Lou et al., 2014). In terms of aerosol's modification on solar radiation, researches explored that ozone production was especially sensitive to aerosol optical depth (AOD)'s increase when solar flux was intense (Ran et al., 2009; Geng et al., 2007; Pozzoli et al., 2011). The photolysis rate of $O_3 \rightarrow O$ was significantly slowed down in lower troposphere when aerosol optical thickness was found to be high (Li et al., 2011). Additionally, the planetary boundary layer (PBL) affected the aerosol and ozone distribution through altering the shape of the lower troposphere (Papayannis et al., 1990). The complex interactions among aerosol–radiation, aerosol–reaction and ozone formation/depletion were quite associated with secondary aerosols (Tao et al., 2014; Lin et al., 2010). Primarily, this uncertainty can be attributed to the blank specific measurement of the aerosol microphysical and optical parameters in ozone-rich environment (Dubovik and King, 2000; Pozzoli et al., 2011).

As a metropolis of the People's Republic of China, Shanghai has a population of 20.6 million in the territory of 6341 km^2 (Shanghai Municipal Statistics Bureau, 2001–2010). With the rapid industrialization and urbanization, Shanghai is undergoing both particulate and ozone pollution (He et al., 2012; Geng et al., 2007). A long-term measurement in Shanghai interpreted ozone as a significant pollutant of surface photochemical oxidant production since the 21st century (Ran et al., 2009). According to the governmental report from Shanghai Environment Monitoring Center (SEMC), ozone as a predominant pollutant accounted for 22.1% and 66.1% days all year round in 2013 and summer of 2013, respectively. Simultaneously, the burden of airborne aerosol has drawn researchers' attentions. He et al. (2012) summarized the seasonal variation of aerosol optical properties in Shanghai, discovering that the highest aerosol loading (~1.20 at 500 nm) occurred in summer. Photo-chemical reactions with secondary particle formation contributed substantially as the aerosol source (Benas et al., 2013; Ding et al., 2008). It further facilitated the impact on the photochemistry and modified the climatological variation (Jenkin and Clemitshaw, 2000; Guo et al., 2012; Li et al., 2013a, 2013b; Yu et al., 2011). Considering the seasonal characteristic and frequent ozone pollution episodes, aerosol optical parameters in summer over Shanghai is of an adequate interest to study on.

Utilizing the data from a ground-based sun-photometer and micro-pulse lidar (MPL), this paper presents AOD, single scattering albedo (SSA), size distribution and vertical profile of extinction ratio during ozone episodes in 2013. As the photochemical reaction took place in daytime with sufficient precursors and solar radiation, ozone always showed dynamic diel variations (Logan, 1985). An analysis on the diurnally varied aerosol optical properties can furtherthe interactions between aerosol and ozone. The experimental data could be applied in sensitivity test for ozone formation and depletion process, in order to improve the accuracy of model simulation (Ran et al., 2009). Additionally, the inverted parameters are original to represent urban/industrial aerosol properties over Shanghai as the measurement is located at a downtown site. The measurement is also indicative of the coagulation, hydroscopic humidification, cloud condensation and gas-to-particle phase conversion process of aerosol (Smirnov et al., 2002).

2. Observation, measurement and case description

2.1. Observational site and measurement

Located at a typical urban area in Shanghai city, the experimental site, Fudan University (FDU, 31°18′N, 121°29′E) is in the convergence of educational, commercial and residential zones without major industrial pollution sources. The Cimel CE-318N sun/sky radiometer was used to obtain aerosol optical parameters. The direct sun calibration was performed in September 2012 at the Izaña Atmospheric Observatory (16° 29′ 57″ W, 28° 18′ 32″ N, 2373 m) with Langley plot analysis, showing about 0.006–0.012 difference of AOD between calibrated and mastering result. The automatic radiometer scans direct sun irradiance and diffused sky radiance four times in an hour at eight spectral channels (340, 380, 440, 500, 675, 870, 1020 and 1640 nm). The algorithm in this study shares the core code of standard one in AERONET (Dubovik and King, 2000). Two parts are different from the classical one in this reliable inversion algorithm: the applications of inter-converting calibration coefficients and a 72-month averaged ground albedo (error ~ 10%) derived from MODIS (details can bee seen in Li et al., 2008, 2013a, 2013b). The retrieved products (including AOD, Ångström exponent (α), size distribution and SSA) were discussed in Section 3.

The micro-pulse lidar (MPL 4B-IDS) in our experiment is an elastic backscatter version developed by NASA Goddard Space Flight Center. Comprising of an optical transceiver unit and rack mounted electronic cell, it has been applied at several locations

worldwide for aerosol and cloud monitoring autonomously (Comstock et al., 2002). The backscattering signals of the MPL are recorded every 15 s and the bin time of the receiver is 200 ns. The vertical spatial resolution of 30 m can be guaranteed while blind range is around 0.25 km. The lidar equation is listed as:

$$P(r) = O_c(r)CE\frac{\beta(r)}{r^2}\exp\left[-2\int_0^r \sigma(z)dz\right]$$

where r represents the detected range, $\beta(r)$ is the total backscattering coefficient while $\sigma(r)$ is the total extinction coefficient. Both of them are comprised of two parts: molecular and aerosol backscattering/extinction coefficients. C is the constant incorporating the transmission and the detection efficiency, and E is the laser pulse energy. $O_c(r)$ is defined as the overlap correction and is a function of the range caused by poor receiver efficiency of the telescope and associated optics in this region. The overlap correction process must be conducted when the MPL is oriented horizontally to measured signal $P_H(r)$:

$$\ln[P_H(r)] = \ln[C\beta] - 2\sigma r + \ln[O_c(r)] = \ln[P_F(r)] + \ln[O_c(r)]$$

where $P_F(r)$ is the linear fit for detected range. Consequently, when detected range is far greater than overlap range, the value of $O_c(r)$ equals to 1. Otherwise it is determined by $P_H(r)/P_F(r)$. As the extinction matters in atmosphere are mainly about aerosol and molecule, the equation can be transformed to:

$$P(r) = O_c(r)CE\frac{[\beta_a(r)+\beta_m(r)]}{r^2}\exp\left[-2\int_0^r [\sigma_a(z)+\sigma_m(z)]dz\right]$$

the subscript a and m denote aerosol and molecule, respectively. To solve the equation, we used Fernald algorithm (Fernald, 1984) to calculate the unknown parameters. As $\beta_m(r)$ and $\sigma_m(z)$ can be obtained according to the National Atmospheric Model, $\beta_a(r)$ and $\sigma_a(z)$ remain to be the target value in calculation. The algorithm defined backscattering ratio $S_a = \sigma_a(z) / \beta_a(r)$ and $S_m = \sigma_m(z) / \beta_m(r)$. The boundary layer height r_m is deemed as upper atmosphere where rare particles could be found. Then aerosol extinction coefficient can be inversed as:

$$\sigma_a(z) = -\frac{S_a}{S_m}\sigma_m(r) + \frac{\ln[P(r)]\exp\left[2\left(\frac{S_a}{S_m}-1\right)\int_r^{r_m}\sigma_m(z)dz\right]}{\frac{\ln P(r_m)}{\sigma_a(r_m)+\frac{S_a}{S_m}\sigma_m(r_m)} + 2\int_r^{r_m}\ln[P(r)]\exp\left[2\left(\frac{S_a}{S_m}-1\right)\int_r^{r_m}\sigma_m(z')dz'\right]}.$$

Particulate matter (PM), nitrogen dioxide (NO_2), sulfate dioxide (SO_2) and carbon monoxide (CO) data were provided by SEMC (http://www.semc.com.cn) and measured with Tapered Element Oscillating Microbalance 1400A monitor, 42i NO–NO_2–NO_x analyzer, 43i SO_2 analyzer and 48i CO analyzer (ThermoFisher Scientific, Co., Ltd., USA), respectively. Meteorological factors (temperature, relative humidity and solar irradiance) were consecutively recorded by CAMS620-HM automatic weather station (Huatron Environment Technology Co., Ltd.) at FDU.

2.2. Ozone pollution episodes in summer 2013 over Shanghai

The North-West Pacific Subtropical High (NWPSH) always exhibits as a prevailing circulation system during monsoon season in East Asia (Zhou et al., 2009). Fig. 1 displays a spatial distribution of temporally averaged geopotential height in East Asia during July and August 2013. The NWPSH (can be distinguished with the constant geopotential line 588 mb in Fig. 1) consecutively facilitated the stable weather with strong downward flow and rare precipitation in a vast area. Consequently, Shanghai experienced an ever-hot summer in 2013. From 1 June to 31 August, the daily highest temperature in 47 days (51%) exceeded 35 °C by the record of Shanghai Meteorological Bureau (http://www.smb.gov.cn). It stimulated the generation of ozone as the temperature is a key factor in photo-chemical reactions (Cheung and Wang, 2005).

According to SEMC (http://www.semc.com.cn), 41 (66.1%) days in July and August 2013 were reported as ozone-polluted days (in Fig. 2a). As shown in Fig. 2(b), the maximum seasonally average O_3 concentration can be discovered in July (~82.6 μg/m^3) when $PM_{2.5}$ (fine particles with aerodynamic diameter less than 2.5 μm) was in a relatively low level (~42.6 μg/m^3). However, by analyzing the hourly data provided by SEMC, the study revealed an interesting phenomenon: $PM_{2.5}$ concentration was positively-correlated with ozone when pollution episodes happened. Fig. 3(a) was depicted to discuss the linear relationship of these two species in clean and ozone polluted cases. The correlation coefficient (R ~ 0.59) in ozone-rich days was obviously higher than clean days (R ~ 0.38), indicating an interaction between particles and O_3 presumably (Bonn and Moorgat, 2002; Ervens et al., 2011; Guo et al., 2012; Chen et al., 2013). As $PM_{2.5}$ was found to be highly correlated with AOD (Xin et al., 2014), a comparative investigation on aerosol characteristics in ozone-polluted and clean conditions is necessary. In case study, AQI (air quality index, identification for prominent pollutant), 8-hour-averaged and maximum (hourly) concentrations of O_3 were used as the threshold to choose two sorts of samples. According to National Ambient Air Quality Standards (GB3095-2012), days with average AQI less than 50 were defined as clean ones (Kan, 2012). Samples with maximum ozone hourly mass concentration >200 μg/m^3 or maximum 8-hour-mean value >100 μg/m^3 were regarded as polluted ones. 21 and 12 daily samples representing ozone polluted and clean days were listed in Table 1. In perspective, four severe ozone-polluted processes (e.g. from 8th to 11th July) occurred in the experimental period. Clean days were found during monsoon and precipitation (e.g. 12th to 14th July and 19th to 22nd August).

3. Results

3.1. Diurnal variation of PM, O_3, and other trace gases in clean and ozone polluted days

Fig. 4 was depicted to illustrate the diurnal variation of gaseous pollutants and particulate matter during ozone episodes and clean condition. In general, the mass concentrations of all pollutants displayed higher values with more dynamic diurnal variations in episodes than clean background. During the ozone polluted events, the diurnal cycle

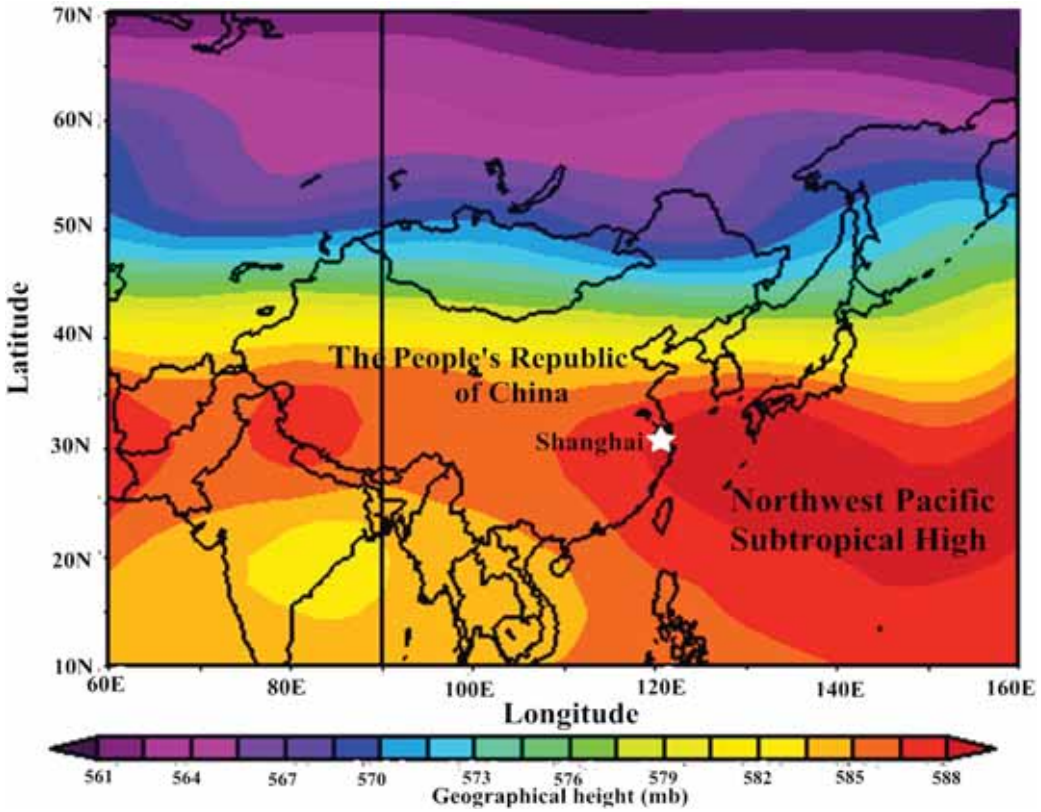

Fig. 1. Spatial distribution of time-averaged geopotential height at 500 mb in East Asia from 1 July to 31 August 2013 derived from NCEP reanalysis data (where the star represents the observation site).

for O_3 presented a single peak (with concentration over 220 μg/m^3 or 111.4 ppbv). The maximum value in this research was approximately 2 times higher than the extreme value (~57 ppbv) measured ten years ago in YRD by Wang et al. (2001), 3.6 times higher than the clean condition (~62.4 μg/m^3). $PM_{2.5}$ biased a bimodal distribution in diurnal variation in Fig. 4(a). The higher concentration of $PM_{2.5}$ in ozone-rich environment may be related to synoptic weather, hygroscopic growth and gas-to-particle conversion (Xin et al., 2014; Chen et al., 2013; Li et al., 2014). Vehicle combustion performed as a principal contributor of nitrogen dioxide (NO_2) and monoxide (NO) in urban area. Hence NO_2 showed high concentration at rush hours with traffic burden. The maximum concentration (~62.3 μg/m^3) occurred at 8 a.m. while the lowest level (~21.7 μg/m^3) was observed after noon. Analogously, the diurnal variation of CO exhibited a double-peak pattern whose high concentration was in rush hours. Note that the higher R (~0.68) in Fig. 3(b) was calculated between $PM_{2.5}$ and CO, which indicated that they were in a similar source. Consistent with NO_x (including NO, NO_2), SO_2 has been proved to exert an essential impact on the formation of secondary aerosol (Zhang et al., 2012; Ervens et al., 2011). The concentration of SO_2 showed its maximum value (~24.9 μg/m^3) at 9 a.m. but descended after noon, which implied its consumption in gas–particle transition process during pollution events (Pozzoli et al., 2011). The lower fitting coefficient (~0.41) between $PM_{2.5}$ and SO_2 during episodes than normal days (~0.56) in Fig. 3(c) also confirmed this assumption (same condition was found between $PM_{2.5}$ and NO_2).

3.2. Diurnal variation of aerosol optical parameters in clean and ozone polluted days

3.2.1. Aerosol optical depth (AOD) and Ångström exponent (α)

Derived from MODIS (Moderate Resolution Imaging Spectrometer) onboard Terra satellite, Fig. 5 presents the seasonal distribution of AOD (at 550 nm) and α in Shanghai region (1° × 1° averaged area in our inversion from 121°E, 31°N to 122°E, 32°N). The four-year-average (2010–2013) AOD approached a unit in the result. And the seasonal values of AOD were in the order: summer > spring > autumn > winter. With the frequent cold front and strong wind, the dispersion condition was well in winter. Hence relatively low AOD (<0.75 in 2010–2013) could be found. Dust from Mongolia and Gobi deserts always invaded East China via long-transport in spring (March, April and May). It would ascend the coarse particle concentration (with small α) and enhance the aerosol optical extinction capability (Yu et al., 2011). During the summer period, though $PM_{2.5}$ concentration in the surface level showed a relatively small value (see in Fig. 2b), elevated α (>1.2) along with heavy aerosol loading (>1) were validated. Uniformly, according to ground-based observation by Xia et al. (2007) and He et al. (2012), maximum AOD was reported in this season (~1.17 in June). We also found that the value spectra of AOD and α in July/August presented wider than other months in Fig. 5. It indicated that the frequency of turbid and clean days both increased during this period. All these implied the complicated characteristics of columnar aerosol in summer, needing a comparative investigation in polluted and clean cases.

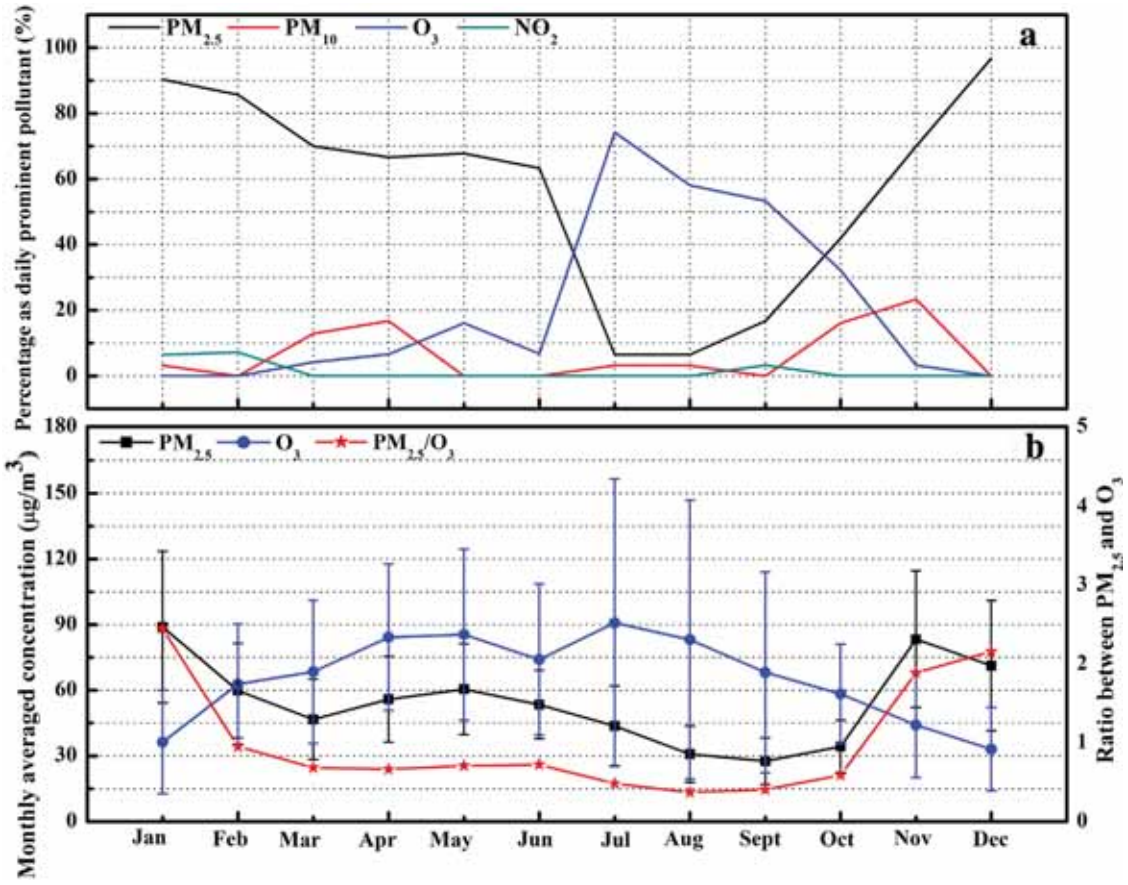

Fig. 2. (a) The variation of prominent pollutant percentages in every month over Shanghai in 2013; (b) monthly average mass concentration[a] of O_3, $PM_{2.5}$ and $O_3/PM_{2.5}$ ratio over Shanghai in 2013 (all data were provided by SEMC, http://www.semc.com.cn).

Fig. 6 showed relatively larger aerosol optical thickness in pollution events (0.79 at 500 nm as daily average) than clean days (~0.32). As we were aware, the turbulence in PBL initiated to run after sunrise. It can elevate gaseous and particulate pollutants from surface layer and enhance aerosol extinction capability in the columnar atmosphere consequently (Papayannis et al., 1990). He and Carmichael (1999) operated a simulation model of ozone mechanism and found that photolysis rates of NO_x would be accelerated when aerosol loadings moderately ascended. In contrast, dimming diurnal fluctuations of AOD (~0.32 in average) was obtained in clean condition. According to the Ångström theory and relevant observations, aerosol insmall size always performed stronger scattering capability (Dubovik et al., 2002). The wavelength index kept an increasing pattern from morning to late afternoon in episode days, during which the largest value (~1.72) appeared at 3 p.m. Studies with scanning electron microscope (SEM) concluded that: during summer in Shanghai, the fine particles comprising of soot aggregates and fly ashes were predominant in ambient air (Lü et al., 2012). Meanwhile, the maximum AOD value (~1.16) along with moderately large α (~1.43) occurred after noon. The secondary aerosols with the diameter less than 0.1 μm was discovered to be an essential production during the photochemical reaction (Bonn and Moorgat, 2002; Guo et al., 2012; Jenkin and Clemitshaw, 2000; Lin et al., 2010). Our result biased the fact that fine particles were gradually formed or accumulated in ozone pollution cases. In contrary, smaller α (~1.02 in average) was discovered in clean samples, signifying the existence of particles with a larger size. This was partially due to the blowing dust and marine aerosol with regional transport (O'Dowd et al., 2010).

As a city cluster with booming urbanization and dense population, urban/industrial aerosol was regarded as a dominant type over YRD (Mi et al., 2007). By this study, the diurnal varied AOD increased from 0.8 to 1.05 (~20%). The result supported the hypothesis that urban/industrial aerosol dominated in this season (Smirnov et al., 2002). AOD along with Ångström exponent can be utilized to further determine the aerosol type (Levy et al., 2007). Fig. 7 displays the scatter plot of hourly-averaged AOD and α in ozone-polluted and clean cases. In non-episode condition, AOD was found to be anti-correlated with α, demonstrating that the aerosol loading was mainly due to large particles (such as dust type). Distinctively, high AOD (>0.85) was almost coupled with relatively large α (>1.2) in ozone episodes. It posed the profound extinction capability of fine particles. During summer over Shanghai, fine particles were usually originated from manufacture facilities, vehicular combustion and secondary formation (He et al., 2012). In ambient air, nitrate, sulfate, ammonium and organic matter could experience

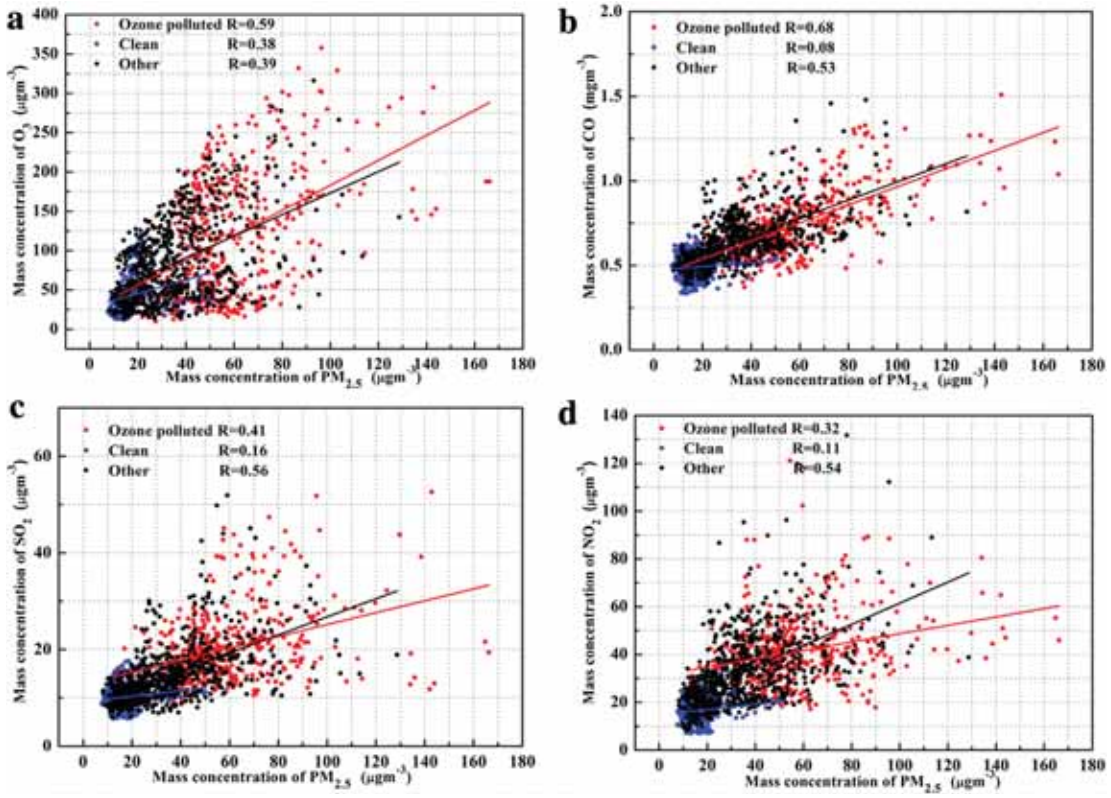

Fig. 3. The scatter-plot of hourly averaged mass concentrations of $PM_{2.5}$ versus (a) O_3, (b) CO, (c) SO_2 and (d) NO_2 over Shanghai in ozone-polluted (red, N = 504), clean (blue, N = 288) and other (black, N = 696) samples in July and August, 2013. (For interpretation of the references to color in this figure legend, the reader is referred to the web version of this article.)

Table 1
The daily AQI (air quality index), mass concentrations[a] of $PM_{2.5}$ (24-hour-mean and hourly maximum) and O_3 (8-hour-mean maximum and hourly maximum) published by SEMC over Shanghai in O_3 polluted days (21) and clean days (12).

Ozone polluted						Clean					
Date	AQI[b]	$PM_{2.5}$ (24 h)	Max $PM_{2.5}$	Max O_3 (8 h)	Max O_3	Date	AQI	$PM_{2.5}$ (24 h)	Max $PM_{2.5}$	Max O_3 (8 h)	Max O_3
1 July	126	99.2	112.5	165.9	223.2	12 July	43	25.6	25.1	56.5	90.4
2 July	121	59.3	65.4	144.0	208.4	13 July	48	18.1	19.9	39.2	50.0
3 July	90	48.9	64.4	120.3	181.1	14 July	49	18.4	21.9	62.8	86.8
4 July	119	50.3	57.7	135.6	187.6	18 July	48	15.9	21.5	70.1	116.1
8 July	120	49.9	62.9	133.6	208.1	19 July	50	17.6	23.2	73.7	115.2
9 July	144	47.9	64.9	162.4	235.4	13 Aug	43	18.6	22.9	59.2	93.3
10 July	150	48.8	60.9	156.1	262.8	14 Aug	43	15.9	20.8	62.8	105.6
11 July	175	51.9	67.6	173.4	293.0	17 Aug	48	18.8	38.2	72.7	99.4
23 July	111	39.6	50.4	131.2	188.5	18 Aug	42	21.4	26.6	31.0	40.3
24 July	121	45.4	60.4	131.3	191.0	19 Aug	50	12.9	23.2	33.5	45.6
25 July	149	52.0	69.7	153.6	235.8	20 Aug	30	12.1	12.9	36.8	56.8
27 July	185	100.8	142.8	180.2	293.9	21 Aug	40	14.8	18.8	45.8	69.0
6 Aug	153	50.1	77.3	178.3	218.7						
7 Aug	207	78.7	89.7	211.9	357.8						
8 Aug	185	103.6	115.5	202.1	279.3						
9 Aug	201	78.4	111.1	229.4	279.9						
10 Aug	157	58.6	78.3	176.9	284.3						
11 Aug	179	74.0	96.3	192.4	303.0						
24 Aug	104	32.1	48.4	127.7	183.4						
29 Aug	120	35.5	56.1	134.3	237.3						
30 Aug	92	75.8	89.9	129.6	163.7						

[a] Mass concentrations of O_3 and $PM_{2.5}$ in this table are in the unit of μg m^{-3}. All data are published by SEMC (website: http://www.semc.com.cn).
[b] Daily AQI was calculated according to the GB3095-2012 put forward by Chinese government; it is used to determine the prominent pollutant; during all ozone polluted days, O_3 is estimated as the prominent pollutant.

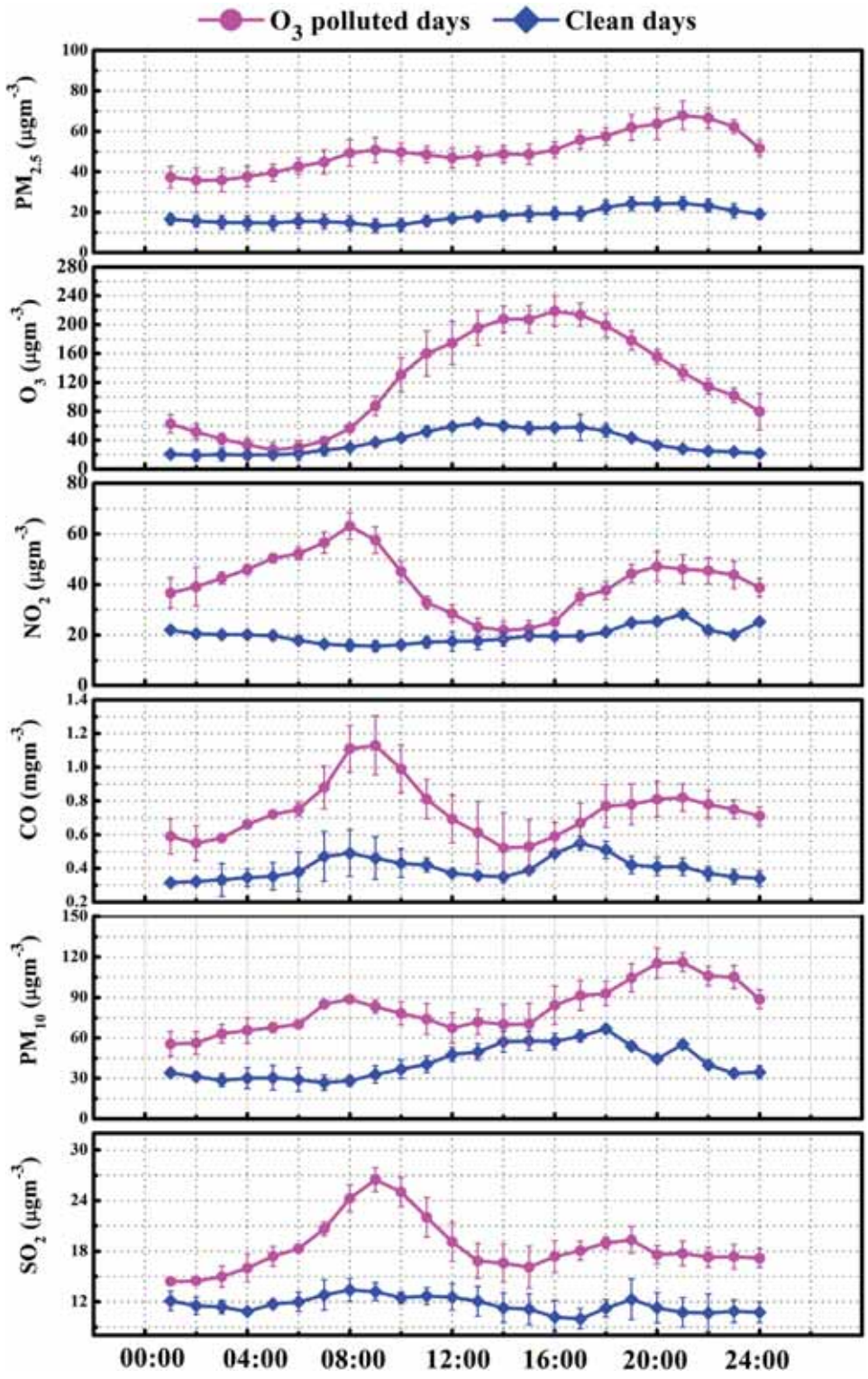

Fig. 4. Diurnal variation of (a).$PM_{2.5}$; (b).O_3; (c).NO_2; (d).CO; (e).PM_{10}; and (f).SO_2 mass concentrations with standard deviations in selected ozone polluted days (21) and clean days (12).

a growth hygroscopic process when humidity was guaranteed. Usually, hydroscopic process can enlarge the particle size while aerosol burden ascends (Li et al., 2014).

3.2.2. Aerosol size distribution

Regarding the wavelength of radiation, aerosol optical properties were discovered to be significantly sensitive to their size and number density (Lin et al., 2010). In order to further investigate the magnitude of aerosol in ozone-polluted days, the authors depicted the size spectra during daytime. In polluted cases, equivalent density (both < 0.07) of coarse and fine particles was observed in early morning. When air turbidity increased, two peaks in bimodal spectra (near 0.15 μm and 4.1 μm) both ascended. The predominance of aerosol in fine

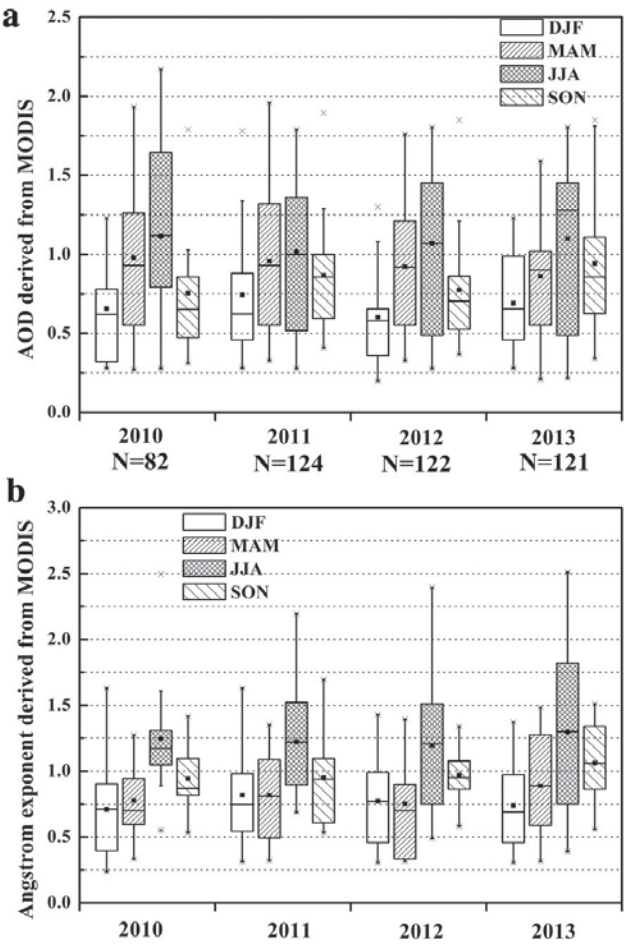

Fig. 5. Seasonally averaged (a).AOD at 550 nm and (b). Ångstrom exponent (α) along with their standard deviations over Shanghai (1° × 1° averaged area in our inversion from 121°E, 31°N to 122°E, 32°N) from 2010 to 2013 derived from MODIS Collection051 products (■ denotes average value).

(including accumulation and Aitken) mode can be explained by: gas–particle transformation/secondary aerosol formation with precursory species (Zuend and Seinfeld, 2012); lower dynamical deposition rates of fine particles than coarse ones. Similar to the rise of AOD around noon, the notable increase of fine particle density at 11 a.m. was shown in Fig. 8. Due to intensive photochemical reactions that always began around 10 to 11 a.m. and particles in photochemical smog pollution were accumulated around 0.002 μm (McMurry and Stolzenburg, 1989), our result may suggest an association with new particle formation (NPF) events (Ervens et al., 2011; Guo et al., 2012; Jenkin and Clemitshaw, 2000). The volume concentration of fine aerosols (peak radius at 0.15 μm) was found to yield a maximum value (~0.28) at 3 p.m. After sunset, the number density of fine particles decreased while concentration in coarse mode increased (~0.08 at 0.15 μm). This was somewhat due to the collapse of PBL and the halt of secondary aerosol formation. Compared to ozone samples, a smooth fluctuation was observed in clean days in regard of their aerosol size distribution (in bottom panel of Fig. 8). The first peak (~0.04 at 0.11 μm) in spectra can be attributed to the vehicle emissions, marine composition, photochemistry products and hygroscopic growth particles. While the second peak (~0.03 at 3.85 μm) was related to blown dust (from city construction fields) and anthropogenic sources (Li et al., 2014; Ervens et al., 2011; O'Dowd et al., 2010).

3.2.3. Aerosol single scattering albedo (SSA)

In Fig. 9(a), the authors presented monthly-averaged SSA derived from sun-photometer in 2013 (some data was unavailable as instrument ceased to work). During July and August, the value decreased from visible spectral to NIR band with weak variation, consistent with the seasonal characteristic recorded in YRD (Xia et al., 2007; Pan et al., 2010). The result also followed the conclusion that aerosol was classified as a non-absorbing type in South-east Asia by Levy et al. (2007). SSA in August was found larger than other months (~0.949 at 440 nm). Uniformly, previous studies in Shanghai have convinced the very scattering characteristic of aerosol in this metropolis, whose SSA in summer exceeded 0.95 in visible band (He et al., 2012). On the other hand, aerosols in well absorption (e.g. black carbon) were considerably reduced as industrial transformation has been implemented in recent years, which increased scattering fraction consequently. Profound scattering effect caused by nitrate and sulfate aerosols may enhance the solar intensity in PBL. It then accelerated the NO_x photolysis rate while increasing ozone formation (Zhang et al., 2012; Papayannis et al., 1990; He and Carmichael, 1999; Li et al., 2011).

As presented in Fig. 9(b), when ozone-polluted episodes occurred, SSA increased continuously from morning (~0.91 at 440 nm for instance) to late afternoon (~0.99). Notably, the in-situ result was larger than the assumed parameter (0.94, 0.68, 0.77 at 400 nm for rural, urban, desert, respectively) in model simulation for ozone mechanism by He and Carmichael (1999). Tao et al. (2014) discovered that ammonium nitrate, ammonium sulfate, organic matter and sea salt were main compositions in aerosol responsible for scattering in urban area. In particular, intensive solar irradiance stimulated dynamic photo-chemical reactions in summertime (daily). It favored the gas–particle conversion and secondary organic aerosol (SOA) formation (Guo et al., 2012; Jenkin and Clemitshaw, 2000). Isoprene facilitated as a critical VOC (volatile organic compounds) species and was modified as a precursor of ozone. Furthermore, isoprene could stimulate the transition of SOA through photo-oxidation (Kroll et al., 2006). As an essential product SOA (optically scattering), isoprene oxidation carbon was found in a far higher concentration during summertime over Shanghai than other seasons (Feng et al., 2013). Meanwhile, SSA in all bands (~0.92 at 440 nm) performed weak diurnal fluctuations when air quality was satisfying. With the largest value (~0.92) observed in the morning, SSA decreased slightly in daytime until the smallest albedo (~0.89) was inversed at twilight. This can be explained by the "sea breeze and land breeze" effect (caused by inhomogeneous heat in land and sea level). However, considering the absolute value (mostly over 0.88) in clean days, the very characteristic of scattering particles was further confirmed in summertime over Shanghai. For a long time, the determination of precise aerosol type with SSA confused the satellite validation (Mi et al., 2007). But it should be noted that the SSA observed in the study can only represent the (urban/industrial) type in Shanghai as temporal and spatial variabilities broadly existed in this area. For the same reason, this parameter was essential and valuable to increase the accuracy of model

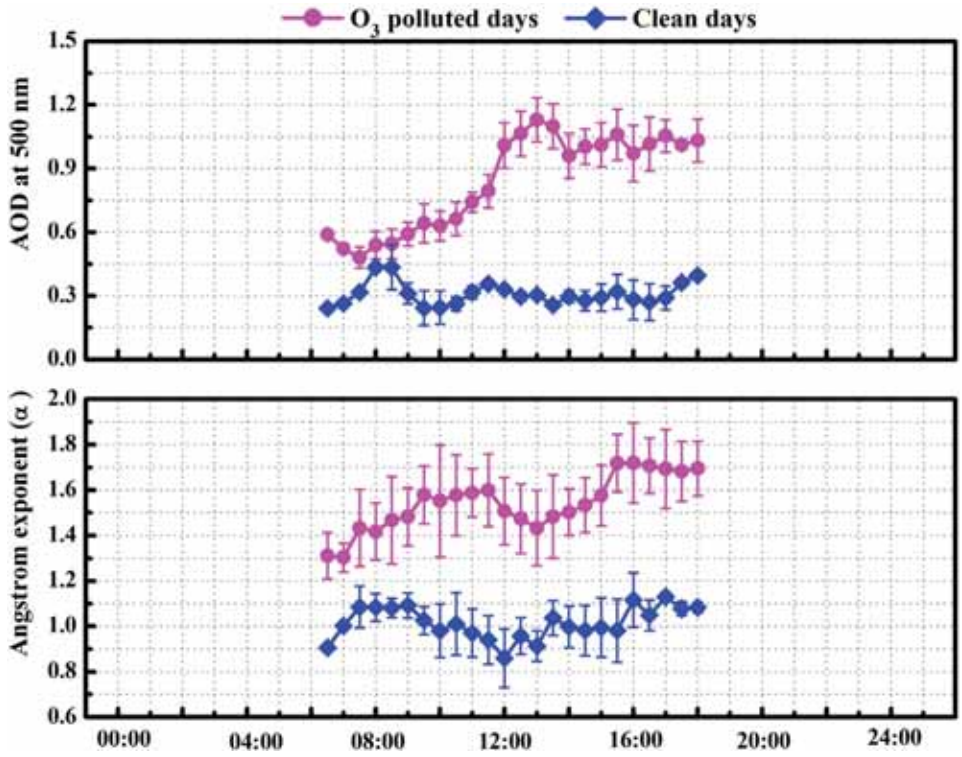

Fig. 6. Diurnal variation of (a).AOD at 500 nm; (b).Ångström exponent selected ozone polluted days (21) and clean days (12) with deviations derived from sun-photometer (all data were half-hourly averaged, e.g. data at 7 a.m. was averaged from 6:45 a.m. to 7:15 a.m.).

simulation for ozone, remote sensing retrievals (He and Carmichael, 1999; Levy et al., 2007).

3.2.4. Vertical profile of aerosol extinction ratio

Lidar was widely applied to observe and retrieve vertical profiles of aerosol extinction/back-scattering ratio (Papayannis et al., 1990). With the MPL measurement, Fig. 10(a,b) showed the diurnal patterns of aerosol extinction profiles and PBL. The dynamic turbulence in PBL began to run as solar radiation heated the earth's surface after sunrise (see in Fig. 10c).

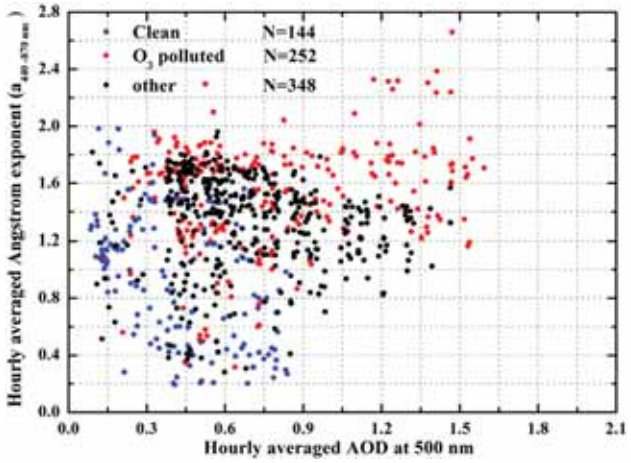

Fig. 7. The scatter-plot of hourly averaged $AOD_{500\ nm}$ and Ångstrom exponent over Shanghai in ozone-polluted (red, N = 252), clean (blue, N = 144) and other (black, N = 348) samples in July and August, 2013. (For interpretation of the references to color in this figure legend, the reader is referred to the web version of this article.)

According to common knowledge, the turbulence can dilute the particulate and gaseous pollutants accumulated in the surface level. However, the interesting phenomenon in our research was presented: the altitude and magnitude of extinction ratio increased up with the developing PBL. The top of PBL in high-concentration ozone environment (~1.96 km) was measured at 3 p.m., when maximum daily temperature was always observed. In ozone episodes, the extreme extinction coefficient (~0.5 km^{-1}) occurred at the altitude of 1.2 km, indicating that ozone formation/photo-chemical reaction was more intensive in the middle PBL. This result agreed well with the former research (Chen et al., 2013), as NO_x (anthropogenic, mainly) in the surface level inhibited the ozone formation process (Benas et al., 2013). An abrupt elevation of extinction ratio was captured after noon (at 1 p.m.) when high temperature, intensive solar radiance, weak horizontal air flow, vigorous convection and sufficient precursors were all guaranteed. It was consistent with the ground-based result by sun-photometer (AOD is the accumulation of extinction ratio in vertical profile). As a significant factor, the turbulence also stimulated the homogeneous distribution of aerosols (Ding et al., 2008). Consequently, scattering aerosols could considerably diffuse the solar radiation and enhance the flux density inside the PBL (He and Carmichael, 1999). In contrast, the shape of extinction profile underwent small changes in daytime when no ozone episode happened. Lower aerosol top illustrated the rather limited development of boundary layer (~1.4 km as maximum at noon), where aerosol extinction capability (~0.1 km^{-1} as maximum) was quite weak (negative values were even observed in morning). On the other hand, hydroscopic growth always increased aerosol loading with relatively high humidity (Li et al., 2014). Though RH was usually low when ozone

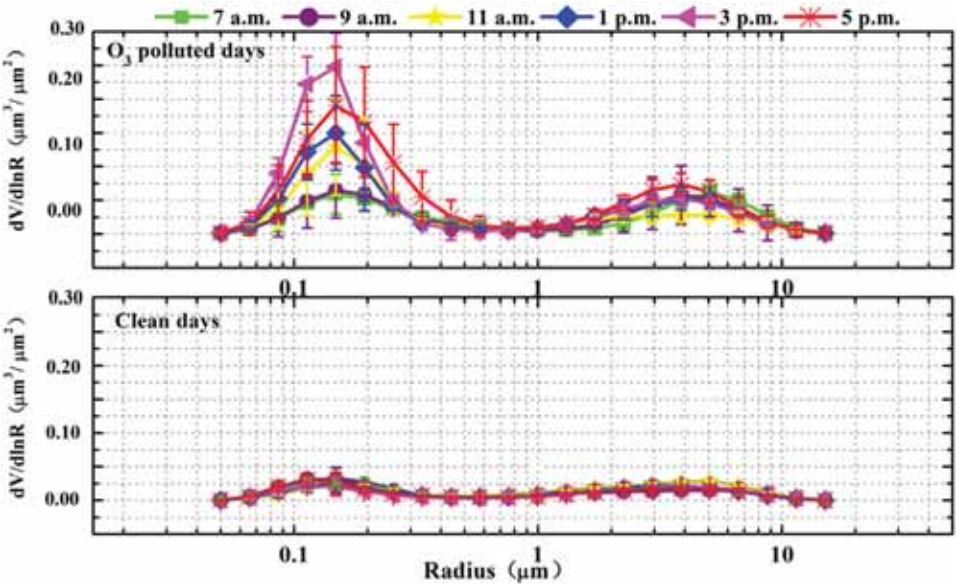

Fig. 8. Diurnal variation of aerosol size distribution in selected ozone polluted days (21) and clean days (12) derived from sun-photometer (all data were two-hourly averaged and in daily time, e.g. data at 7 a.m. was averaged from 6 a.m. to 8 a.m.).

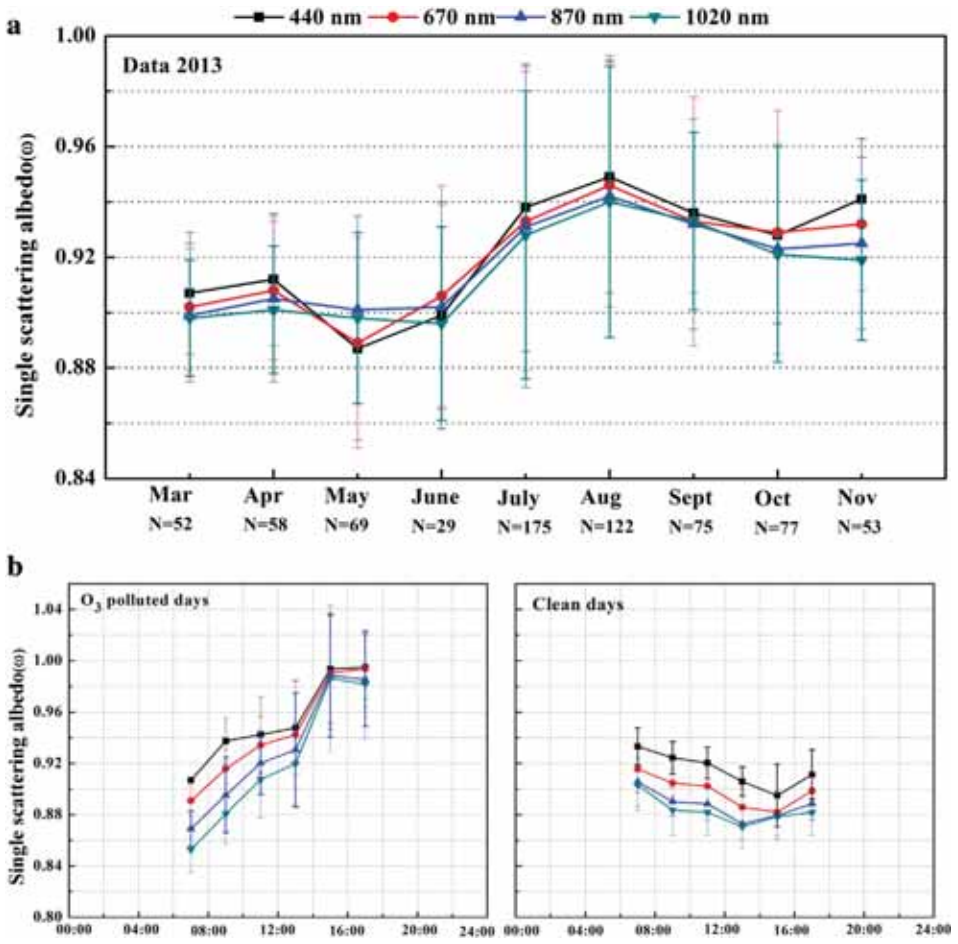

Fig. 9. (a) Monthly averaged of single scattering albedo (SSA) at four wavelengths at FDU since March to November in 2013; (b) diurnal variation of single scattering albedo at 440,670,870 and 1020 nm in selected ozone polluted (21) days and clean (12) days derived from sun-photometer (data was two-hourly averaged in daily time).

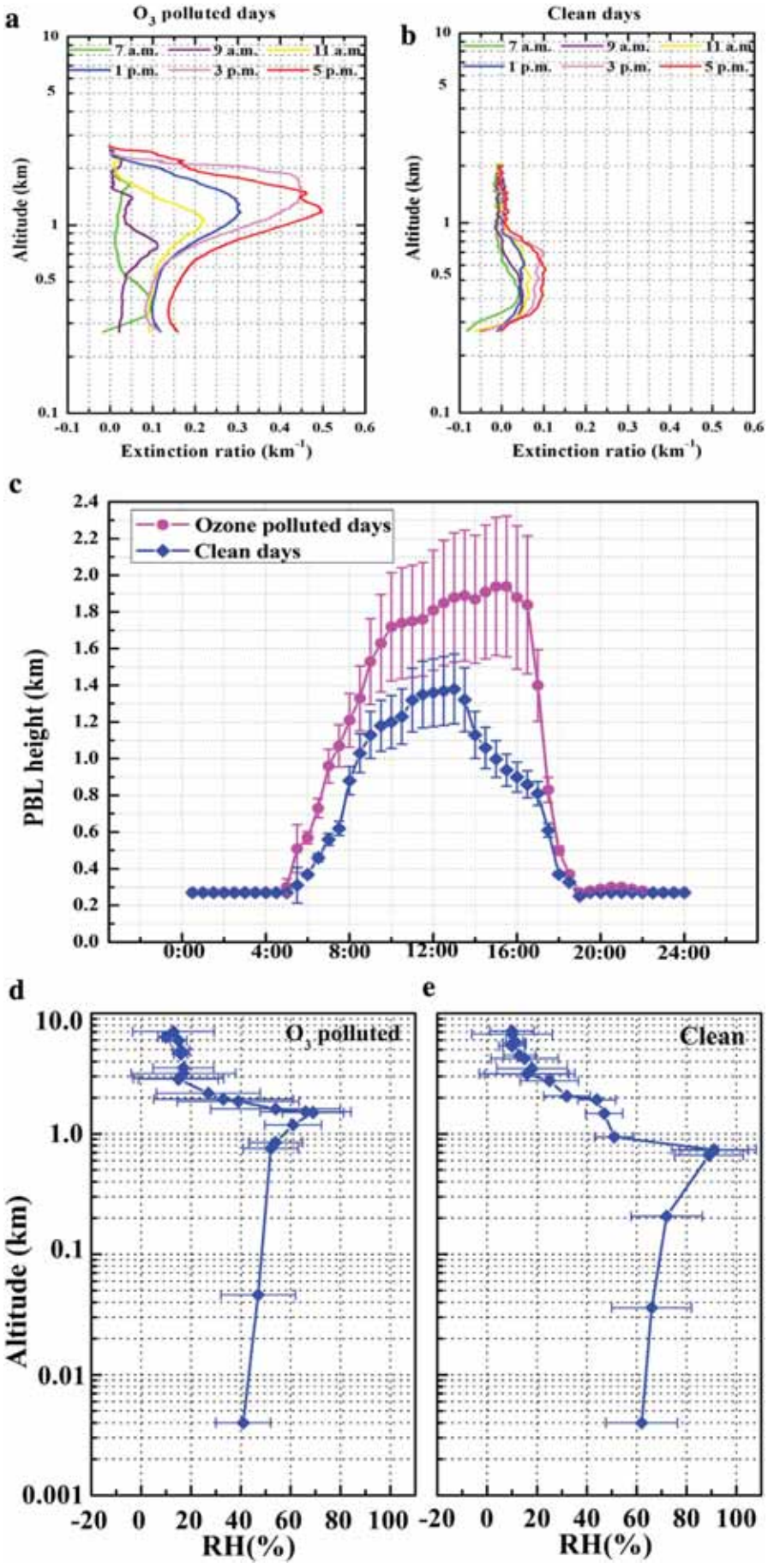

Fig. 10. Diurnal variation of (a,b) vertical profile of aerosol extinction ratio, (c) boundary layer (blind range is 0.25 km) derived from the MPL and (d,e) vertical profile of relative humidity (at 12 UTC, sounding data from website: http://www.weather.uwyo.edu/upperair/sounding.html) in selected ozone polluted days (21) and clean days (12).

pollution occurred (see in Fig. 11c), itmay permit the hydroscopic process. Phenomenally, through the RH profiles by atmospheric sounding (http://www.weather.uwyo.edu/upperair/sounding.html), we found that the maximum values were presented at 1.4 km and 0.8 km for ozone-polluted and clean condition, respectively. Considering the almost same altitude of extreme extinction ratio occurrence, the strong optical extinction effect may be a result from both photochemical and hydroscopic activities.

The unprecedented ozone concentration (357.8 μg/m^3) was monitored in 7 August, which granted us an opportunity to operate a specific investigation. The ambient temperature (~40.8 °C) in this day broke out the historical record since 1871. Strong temporal variation with extremely high extinction coefficients was reproduced in Fig. 11(c). The maximum layer top (~2.7 km) and extinction coefficient (0.5 km^{-1}) at the height of 1.5 km was observed around 4 p.m. Both ozone concentration and PBL height decreased acutely after sunset. Combining with the meteorological elements in Fig. 11(d), it implied that dry air flow with potent convection consecutively developed in PBL. It then resulted in the necessary heat, well-mixed scattering aerosols and ozone precursors. These all vigorously stimulated the substantial ozone formation in aerosol-rich environment (He and Carmichael, 1999). Besides, we found that the diurnal pattern of ozone, temperature and aerosol extinction profile shared large similarities. In contrast, 18 Aug represented the clean condition in Fig. 11(a,b). All parameters therein were lower than the polluted ones. Backward air flow analysis based on HYSPLIT (hybrid single-particle Lagrangian integrated trajectory) was performed in Fig. 12. It is well-known that during monsoon season, sea-wind would bring about clean air-flow to Shanghai. In comparison, ozone days were featured with the air flow from inland (hot and dry), which favored the photo-chemical reaction. The lower air flow speed also implied the worse diffusion condition. Particulate and gaseous pollutants can be accumulated. Additionally, the regional transport (inland wind) may also contribute to the particles and ozone pollution from the city clusters over YRD.

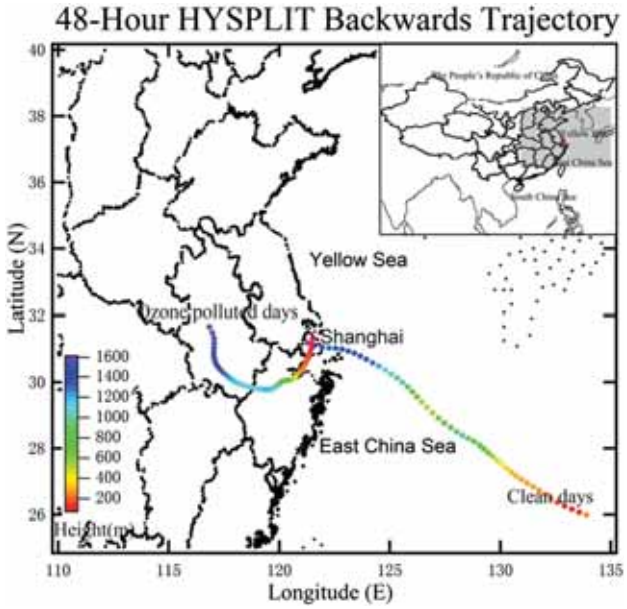

Fig. 12. 48-hour air backward trajectories based on HYSPLIT model for ozone days and clean days (the two types of trajectories were averaged with 21 and 12 samples respectively).

4. Discussions

Till now, the (positive or negative) impact of aerosols on ozone remains to be an uncertain issue while studies showed different conclusions (Lou et al., 2014; Pozzoli et al., 2011; Wang et al., 2001; Liao and Seinfeld, 2005). Generally, it is well agreed that there are two processes concerning the aerosol–ozone interactions: modifying heterogeneous reaction and altering photolysis rate (Hofmann et al., 1994; Jenkin and Clemitshaw, 2000). In regardto heterogeneous reaction, it was revealed that the uptake of NO_x by columnar aerosol (especially at noon) could increase 1–14% O_3 in VOC-limited region (Xu et al., 2012). Meanwhile, it was concluded that the

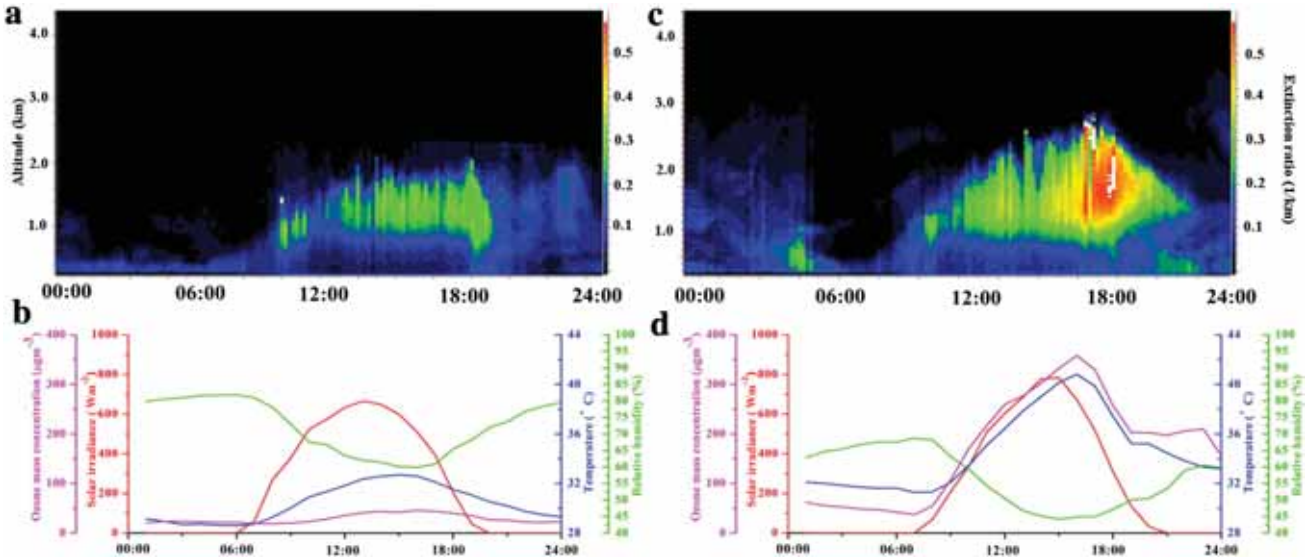

Fig. 11. Diel variation of vertical profile of aerosol extinction ratio, mass concentration of O_3, temperature, solar irradiance and relative humidity in 18 Aug (clean, left panel) and 7 Aug (ozone-polluted, right panel).

absorption of NO_3, NO_2 could increase OH radicals, consequently leading to ozone increases in all seasons (Lou et al., 2014). This phenomenon was especially observed in eastern China with severe particle pollution. Hence the heterogeneous reaction could stimulate the ozone formation in daytime during summertime (Ran et al., 2009), which may also exist in our observation. But on the opposite side, it was uncovered that surface ozone concentrations in eastern China was reduced by 25–30% due to heterogeneous reactions on sulfate, nitrate, ammonium, OC, sea salt, and mineral dust aerosols (Liao and Seinfeld, 2005). In terms of the photolysis rate, He and Carmichael (1999) found that scattering aerosol would diffuse the solar radiation and increase the flux intensity inside boundary layer (see solar irradiance in Fig. 11b,d). It then increased the photolysis rate of surface NO_x when the aerosol loading was not very heavy (high AOD would penetrate radiation in aerosol layer). However, some researchers found that surface-layer photolysis rates $J(O_3)$ and $J(NO_2)$ would be reduced by 20–30% and 10–30% in winter as well as 5–20% and 1–10% in summer (Tie et al., 2005). Consequently, reductions in surface-layer O_3 concentrations by 2–4% in winter and less than 1% in summer could be simulated.

To further explain and these contracted results, subsequent experiments including in-situ and model simulation should be addressed then. This facilitated as a merit of this study as it may offer a possible way to comprehend the complicated field. Defined as the ratio of change in ozone concentration ($\triangle O_3$) to local $PM_{2.5,}$ ROP ($\triangle O_3/PM_{2.5}$) can be calculated to estimate the aerosol impacts on ozone variation. The calculation turned out to be 0.09 in this study (ozone-polluted samples), confirming the positive relation between aerosol and ozone. As neither AOD (~0.78 as average) nor $PM_{2.5}$ concentration in our research presented very high values (in ozone pollution events), the considerable scattering feature (see in Fig. 9) may decrease $J(O_3)$ while it stimulates $J(NO_2)$, increasing the ozone formation consequently. The scattering capability was determined by the AOD $*$ SSA, hence a positive correlation can be found between AOD and ozone concentration.

5. Conclusions

Utilizing the sun-photometer and MPL, this paper aimed to analyze the aerosol optical properties in ozone-rich environment while it discusses the impacts of aerosol on ozone preliminarily. Seasonal result derived from MODIS showed that the heaviest aerosol loading (>1.0 at 550 nm) occurred in summer over Shanghai. Simultaneously, maximum surface ozone concentration (82.6 μg m^{-3}) was found during this season. Furthermore, a positive-correlation (R ~ 0.59) was unfolded between $PM_{2.5}$ and O_3 concentrations in ozone-polluted condition. Contrary to expectations, this study also revealed that the heavy aerosol loading was well-correlated with O_3 generation during ozone pollution episodes. AOD (at 500 nm) in ozone-polluted days (~0.78) was presented to be 2.4 times higher than clean days (~0.32). Increasing trend of daily varied Ångström exponent (~1.51 as average) biased the formation and accumulation of fine particles. AOD along with Ångström exponent indicated a considerable optical extinction caused by fine aerosol. The dynamic diurnal variation of these parameters implied a complex interaction between aerosols and photo-chemical reactions. Unfavorable meteorological condition (with slow air flow) permitted the diffusion of pollutants, which facilitated as another factor increasing aerosol loading. The positive correlation between aerosol and ozone in this research may be attributed to two parts. Firstly, the absorption of NO_x by aerosols (in heterogeneous reactions) could lead to ozone increases in VOC-limited region. In this study, as aerosol loading was not extremely high, scattering aerosol exerted a stimulating role in ozone formation through increasing solar flux in aerosol layer.

The bimodal pattern for aerosol size distribution was presented in both ozone and clean days. Particles in fine mode (radius < 0.6 μm) were posed to be dominant in ozone-rich environment. In diurnal cycle, the extreme concentration (~0.28) of aerosol in fine mode occurred at 3 p.m. (local time) in episodes. In contrast, a smooth fluctuation with small volume concentration (~0.03 and ~0.02 in fine and coarse modes as maximum) was retrieved in clean days. SSA ascended continuously from morning (~0.91 at 440 nm) to late afternoon (~0.99 at 4 p.m.) when ozone was substantially generated. Dynamic photo-chemical reactions in summertime favored the gas–particle conversion (for ammonium nitrate, ammonium sulfate etc.) and SOA formation, which enhanced the feature of scattering consequently. The gradually increasing SSA and fine particle (number) density during daytime suggested a presumable association with the NPF event. With the MPL, we found that both the altitude and magnitude of maximum extinction ratio increased with the developing PBL. The top height of PBL was observed to be 1.96 km and 1.4 km in ozone polluted and clean condition, respectively. The maximum value (~0.5 km^{-1}) was explored at the height of 1.2 km in late afternoon (at 5 p.m.), when ozone episodes occurred. Interestingly, through the sounding data of RH profiles, we found that the maximum values were presented at 1.4 km and 0.8 km for ozone-polluted and clean condition. In regard to the almost the same altitude of extreme RH and extinction ratio occurrence, the strong optical extinction effect may be a result from both photochemical and hydroscopic activities.

Acknowledgments

This study was financially supported by the National Natural Science Foundation of China under Grant no. 21277029, 40975076, 41365010, the Science and Technology Commission of Shanghai Municipality (Grant: 12DJ1400102), and China Meteorological Administration (Grant: GYHY201106045-8). We also gratefully appreciate the support of National Hightech R&D Program ("863" Program, No. 2006AA06Z417). Sincere thanks belong to the MODIS team for its talented products. Great thanks owe to the NOAA Air Resources Laboratory (ARL) for provision of the HYSPLIT trajectory model for public use. We also would like to extend our respects to Shanghai Environmental Monitoring Center for the immediate publication of AQI data.

References

Benas, N., Mourtzanou, E., Kouvarakis, G., Bais, A., Mihalopoulos, N., Vardavas, I., 2013. Surface ozone photolysis rate trends in the Eastern Mediterranean: modeling the effects of aerosols and total column ozone based on Terra MODIS data. Atmos. Environ. 74, 1–9.

Bonn, B., Moorgat, G.K., 2002. New particle formation during alpha-and beta-pinene oxidation by O_3, OH and NO_3, and the influence of water vapour: particle size distribution studies. Atmos. Chem. Phys. 2, 183–196.
Chen, P.F., Quan, J.N., Zhang, Q., Tie, X.X., Gao, Y., Li, X., Huang, M.Y., 2013. Measurements of vertical and horizontal distributions of ozone over Beijing from 2007 to 2010. Atmos. Environ. 74, 37–44.
Cheung, V.T., Wang, T., 2005. Observational study of ozone pollution at a rural site in the Yangtze Delta of China. Atmos. Environ. 35, 4947–4958.
Comstock, J.M., Ackerman, T.P., Mace, G.G., 2002. Ground-based lidar and radar remote sensing of tropical cirrus clouds at Nauru Island: cloud statistics and radiative impacts. J. Geophys. Res. 107, AAC 16.
Ding, A.J., Wang, T., Thouret, V., Cammas, J.P., Nédélec, P., 2008. Tropospheric ozone climatology over Beijing: analysis of aircraft data from the MOZAIC program. Atmos. Chem. Phys. 8, 1–13.
Dubovik, O., King, M.D., 2000. A flexible inversion algorithm for retrieval of aerosol optical properties from sun and sky radiance measurements. J. Geophys. Res. 105, 20673–20696.
Dubovik, O., Holben, B., Eck, T.F., Smirnov, A., Kaufman, Y.J., King, M.D., Tanré, D., Slutsker, I., 2002. Variability of absorption and optical properties of key aerosol types observed in worldwide locations. J. Atmos. Sci. 59, 590–608.
Ervens, B., Turpin, B.J., Weber, R.J., 2011. Secondary organic aerosol formation in cloud droplets and aqueous particles (aqSOA): a review of laboratory, field and model studies. Atmos. Chem. Phys. 11, 11069–11102.
Feng, J.L., Li, M., Zhang, P., Gong, S.Y., Zhong, M., Wu, M.H., Zhong, M., Chen, C.H., Wang, H.L., Lou, S.R., 2013. Investigation of the sources and seasonal variations of secondary organic aerosols in $PM_{2.5}$ in Shanghai with organic tracers. Atmos. Environ. 79, 614–622.
Fernald, G., 1984. Analysis of atmospheric lidar: some comments. Appl. Opt. 23, 652–653.
Geng, F.H., Zhao, C.S., Tang, X., Lu, G.L., Tie, X.X., 2007. Analysis of ozone and VOCs measured in Shanghai: a case study. Atmos. Environ. 41, 989–1001.
Guo, H., Wang, D.W., Cheung, K., Ling, Z.H., Chan, C.K., Yao, X.H., 2012. Observation of aerosol size distribution and new particle formation at a mountain site in subtropical Hong Kong. Atmos. Chem. Phys. 12, 9923–9939.
He, S., Carmichael, G.R., 1999. Sensitivity of photolysis rates and ozone production in the troposphere to aerosol properties. J. Geophys. Res. 104, 26307–26324.
He, Q.S., Li, C.C., Geng, F.H., Yang, H.Q., Li, P.R., Li, T.T., Liu, D.W., Pei, Z., 2012. Aerosol optical properties retrieved from sun photometer measurements over Shanghai. J. Geophys. Res. 117 (D16204).
Hofmann, D.J., Oltmans, S.T., Komhyr, W.D., Harris, J.M., Lathrop, J.A., Langford, A.O., Deshler, T., Johnson, B.J., Torres, A., Matthews, W.A., 1994. Ozone loss in the lower stratosphere over the United States in 1992–1993: evidence for heterogeneous chemistry on the Pinatubo aerosol. Geophys. Res. Lett. 21, 65–68.
IPCC, 2001. Climate Change 2001: the Scientific Basis-contribution of Working Group I to the Third Assessment Report of the Intergovernmental Panel on Climate Change. Cambridge University Press, New York.
Jacobson, M.Z., 1998. Studying the effects of aerosols on vertical photolysis rate coefficient and temperature profiles over an urban airshed. J. Geophys. Res. 103 (10593–10510).
Jenkin, M.E., Clemitshaw, K.C., 2000. Ozone and other secondary photochemical pollutants: chemical processes governing their formation in the planetary boundary layer. Atmos. Environ. 34, 2499–2527.
Kan, H.D., 2012. A review of standard value of fine particulate matter ($PM_{2.5}$) ruled by National Ambient Air Quality Standards (GB3095-2012) in China. Chin. J. Prev. Med. 46, 396–398.
Kroll, J.H., Ng, N.L., Murphy, S.M., Flagan, R.C., Seinfeld, J.H., 2006. Secondary organic aerosol formation from isoprene photooxidation. Environ. Sci. Technol. 40, 1869–1877.
Levy, R.C., Remer, L.A., Mattoo, S., Vermote, E.F., Kaufman, Y.J., 2007. Second-generation operational algorithm: retrieval of aerosol properties over land from inversion of Moderate Resolution Imaging Spectroradiometer spectral reflectance. J. Geophys. Res. 112 (D13211).
Li, Z.Q., Blarel, L., Podvin, T., Goloub, P., Buis, J.P., Morel, J.P., 2008. Transferring the calibration of direct solar irradiance to diffuse-sky radiance measurements for CIMEL sun-sky radiometers. Appl. Opt. 47, 1368–1377.
Li, J., Wang, Z., Wang, X., Yamaji, K., Takigawa, M., Kanaya, Y., Pochanart, P., Liu, Y., Irie, H., Hu, B., Tanimoto, H., Akimoto, H., 2011. Impacts of aerosols on summertime tropospheric photolysis frequencies and photochemistry over Central Eastern China. Atmos. Environ. 45 (10), 1817–1829.
Li, L., Chen, J.M., Wang, L., Melluki, W., Zhou, H.R., 2013a. Aerosol single scattering albedo affected by chemical composition: an investigation using CRDS combined with MARGA. Atmos. Res. 124, 149–157.
Li, Z., Gu, X., Wang, L., Li, D., Xie, Y., Li, K., Dubovik, O., Schuster, G., Goloub, P., Li, Y., Li, Z., Ma, Y., Xu, H., 2013b. Aerosol physical and chemical properties retrieved from ground-based remote sensing measurements during heavy haze days in Beijing winter. Atmos. Chem. Phys. 13, 10171–10183.
Li, J.W., Han, Z.W., Zhang, R.J., 2014. Influence of aerosol hygroscopic growth parameterization on aerosol optical depth and direct radiative forcing over East Asia. Atmos. Res. 140–141, 14–27.
Liao, H., Seinfeld, J.H., 2005. Global impacts of gas-phase chemistry aerosol interactions on direct radiative forcing by anthropogenic aerosols and ozone. J. Geophys. Res. 110 (D18208).
Lin, J., Nielsen, C.P., Zhao, Y., Lei, Y., Liu, Y., McElroy, M.B., 2010. Recent changes in particulate air pollution over China observed from space and the ground: effectiveness of emission control. Environ. Sci. Technol. 44, 7771–7776.
Lippmann, M., 1995. Health effects of tropospheric ozone. Environ. Sci. Technol. 25, 1954–1962.
Logan, J.A., 1985. Tropospheric ozone: seasonal behavior, trends, and anthropogenic influence. J. Geophys. Res. 90, 10463–10482.
Lou, S.J., Liao, H., Zhu, B., 2014. Impacts of aerosols on surface-layer ozone concentrations in China through heterogeneous reactions and changes in photolysis rates. Atmos. Environ. 85, 123–138.
Lü, S.L., Zhang, R., Yao, Z.K., Yi, F., Ren, J.J., Wu, M.H., Feng, M., Wang, Q.Y., 2012. Size distribution of chemical elements and their source apportionment in ambient coarse, fine, and ultrafine particles in Shanghai urban summer atmosphere. J. Environ. Sci. 24, 882–890.
McMurry, P.H., Stolzenburg, M.R., 1989. On the sensitivity of particle size to relative humidity for Los Angeles aerosols. Atmos. Environ. 23, 497–507.
Mi, W., Li, Z.Q., Xia, X.G., Holben, B., Levy, R., Zhao, F.S., Chen, H.B., Cribb, M., 2007. Evaluation of the moderate resolution imaging spectroradiometer aerosol products at two aerosol robotic network stations in China. J. Geophys. Res. 112 (D22S08).
O'Dowd, C.D., Smith, M.H., Consterdine, I.E., Lowe, J.A., 2010. Marine aerosol, sea-salt, and the marine sulphur cycle: a short review. Atmos. Environ. 31 (1), 73–80.
Pan, L., Che, H.Z., Geng, F.H., Xia, X.G., Wang, Y.Q., Zhu, C.Z., Chen, W., Gao, J., Guo, J.P., 2010. Aerosol optical properties based on ground measurements over the Chinese Yangtze Delta Region. Atmos. Environ. 44 (21), 2587–2596.
Papayannis, A., Ancellet, G., Pelon, J., Megie, G., 1990. Multiwavelength lidar for ozone measurements in the troposphere and the lower stratosphere. Appl. Opt. 29, 467–476.
Pozzoli, L., Janssens-Maenhout, G., Diehl, T., Bey, I., Schultz, M., Feichter, J., Vignati, E., Dentener, F., 2011. Re-analysis of tropospheric sulfate aerosol and ozone for the period 1980–2005 using the aerosol-chemistry-climate model ECHAM5-HAMMOZ. Atmos. Chem. Phys. 11, 9563–9594.
Ran, L., Zhao, C.S., Geng, F.H., Tie, X.X., Tang, X., Peng, L., Zhou, G.Q., Yu, Q., Xu, J.M., Guenther, A., 2009. Ozone photochemical production in urban Shanghai, China: analysis based on ground level observations. J. Geophys. Res. 114 (D15301).
Shanghai Municipal Statistics Bureau, 2001–2010. Shanghai Statistical Yearbook 2001–2010. China Stat, Beijing, China.
Smirnov, A., Holben, B.N., Eck, T.F., Slutsker, I., Chatenet, B., Pinker, R.T., 2002. Diurnal variability of aerosol optical depth observed at AERONET (Aerosol Robotic Network) sites. Geophys. Res. Lett. 29, 30–31.
Tao, J., Zhang, L.M., Ho, K.F., Zhang, R.J., Li, Z.J., Zhang, Z.S., Lin, M., Cao, J.J., Liu, S.X., Wang, G.H., 2014. Impact of $PM_{2.5}$ chemical compositions on aerosol light scattering in Guangzhou—the largest megacity in South China. Atmos. Res. 136–136, 48–58.
Thurston, G.D., Ito, K., 2000. Epidemiological studies of acute ozone exposures and mortality. J. Expo. Anal. Environ. Epidemiol. 11, 286–294.
Tie, X.X., Madronich, S., Walters, S., Edwards, D.P., Ginoux, P., Mahowald, N., Zhang, R.Y., Lou, C., Brasseur, G., 2005. Assessment of the global impact of aerosols on tropospheric oxidants. J. Geophys. Res. 110 (D03204).
Varotsos, C., 2005. Airborne measurements of aerosol, ozone, and solar ultraviolet irradiance in the troposphere. J. Geophys. Res. 110 (D09202).
Wang, T., Cheung, V.T.F., Anson, M., Li, Y.S., 2001. Ozone and related gaseous pollutants in the boundary layer of eastern China: overview of the recent measurements at a rural site. Geophys. Res. Lett. 28, 2373–2376.
Xia, X.G., Li, Z.Q., Holben, B., Wang, P., Eck, T., Chen, H.B., Cribb, M., Zhao, X.Y., 2007. Aerosol optical properties and radiative effects in the Yangtze Delta region of China. J. Geophys. Res. 112 (D22S12).
Xin, J.Y., Zhang, Q., Wang, L.L., Gong, C.S., Wang, Y.S., Liu, Z.R., Gao, W.K., 2014. The empirical relationship between the $PM_{2.5}$ concentration and aerosol optical depth over the background of North China from 2009 to 2011. Atmos. Res. 138, 179–188.
Xu, J., Zhang, Y.H., Zheng, S.Q., He, Y.J., 2012. Aerosol effects on ozone concentrations in Beijing: a model sensitivity study. J. Environ. Sci. 24, 546–656.
Yu, X.N., Zhu, B., Yin, Y., Yang, J., Li, Y.W., Bu, X.L., 2011. A comparative analysis of aerosol properties in dust and haze–fog days in a Chinese urban region. Atmos. Res. 99, 241–247.
Zhang, H., Shen, Z., Wei, X., Zhang, M., Li, Z., 2012. Comparison of optical properties of nitrate and sulfate aerosol and the direct radiative forcing due to nitrate in China. Atmos. Res. 113, 113–125.
Zhou, Y., Savijärvi, H., 2014. The effect of aerosols on long wave radiation and global warming. Atmos. Res. 135, 102–111.

Zhou, T.J., Yu, R.C., Zhang, J., Drange, H., Cassou, C., Deser, C., Hodson, D.L., Sanchez-Gomez, E., Li, J., Keenlyside, N., 2009. Why the western Pacific subtropical high has extended westward since the late 1970s. J. Clim. 22, 2199–2215.

Zuend, A., Seinfeld, J., 2012. Modeling the gas–particle partitioning of secondary organic aerosol: the importance of liquid–liquid phase separation. Atmos. Chem. Phys. 12, 3857–3882.